SAND2011-7246C

MEGAAMPS, MEGAGAUSS, AND MEGABARS: USING THE SANDIA Z MACHINE TO PERFORM EXTREME MATERIAL DYNAMICS EXPERIMENTS

Marcus D. Knudson

Sandia National Laboratories[*]*, Albuquerque NM 87123*

Abstract. For the past decade, a large, interdisciplinary team at Sandia National Laboratories has been refining the Z Machine (20+ MA and 10+ MGauss) into a mature, robust, and precise platform for material dynamics experiments in the multi-Mbar pressure regime. In particular, significant effort has gone into effectively coupling condensed matter theory, magneto-hydrodynamic simulation, and electromagnetic modeling to produce a fully self-consistent simulation capability able to very accurately predict the performance of the Z machine and various experimental load configurations. This capability has been instrumental in the ability to develop experimental platforms to routinely perform magnetic ramp compression experiments to over 4 Mbar, and magnetically accelerate flyer plates to over 40 km/s, creating over 20 Mbar impact pressures. Furthermore, a strong tie has been developed between the condensed matter theory and the experimental program. This coupling has been proven time and again to be extremely fruitful, with the capability of both theory and experiment being challenged and advanced through this close interrelationship. This paper will provide an overview of the material dynamics platform and discuss several examples of the use of Z to perform extreme material dynamics studies with unprecedented accuracy in support of basic science, planetary astrophysics, inertial confinement fusion, and the emerging field of high energy density laboratory physics.

Keywords: Ramp and shock compression, equation of state, tantalum, quartz, beryllium, diamond.
PACS: 07.35.+k, 64.30.-t, 62.50.-p, 62.50.Ef.

INTRODUCTION

The Z accelerator [1] is a low inductance pulsed power generator capable of capacitively storing ~22 MJ of electrical energy. In the configuration used for material dynamics experiments, the machine utilizes a combination of fast switches and transmission lines to deliver up to ~25 MA, ~300-800 ns rise-time current pulse to a short circuit load at the center of the accelerator. This pulse generates a time-varying magnetic field in the anode-cathode (AK) gap of the short circuit. The subsequent Lorentz force generated by these high currents and magnetic fields produces magnetic compression of the cathode and anode over the discharge time of the accelerator [2]. At the highest levels, currents of ~26 MA, magnetic fields of ~10 MGauss, and magnetic pressures of ~600 GPa can be produced for use in dynamic material properties experiments.

[*] Sandia National Laboratories is a multiprogram laboratory managed and operated by Sandia Corporation, a wholly owned subsidiary of Lockheed Martin Company, for the US Department of Energy's National Nuclear Security Administration under Contract No. DE-ACO4-94AL85000.

Two different short circuit geometries are routinely used in materials testing, as shown in Fig. 1. The first of these is a coaxial geometry, in which four anode panels surround a rectangular cathode stalk. This geometry benefits in that the magnetic field is fully confined within the anode assembly. However, this geometry requires that the magnetic field be uniform along the length of the load, or between panels, to allow for accurate inference of the isentrope – a requirement difficult to satisfy with the small AK gaps necessary to reach high peak stresses. The second is a stripline geometry, in which a cathode panel extends through an opening in the upper anode plate of the machine, and stands opposite an anode panel. This geometry allows for samples to be mounted on both the anode and cathode, enabling the same magnetic field to drive two different samples. However, this geometry introduces three-dimensional effects that become important, which will be discussed later.

In addition to varying the short circuit geometry, the current density for a given geometry can be altered by adjusting the charge voltage of the accelerator. Since the peak current scales approximately linearly with the charge voltage, the magnetic pressure can be reduced by as much as ~45% using this approach. These two parameters, the geometry and the charge voltage, allow the peak magnetic pressure to be continuously varied from a few tenths of a GPa to several hundreds of GPa.

These types of loads have been used to develop two experimental platforms. Firstly, the magnetic pressure can be applied directly to samples of interest, resulting in ramp compression [2]. In this way, multiple samples of differing thickness can be ramp loaded to peak stresses of ~400-500 GPa, enabling determination of the pressure-density response of the material along a quasi-isentrope. Secondly, the magnetic pressure can be used as an impulse to launch nearly ambient state flyer plates to velocities exceeding 40 km/s [3]. Impact experiments using this technique enable access to extremely high pressure along the Hugoniot, exceeding 20 Mbar for high impedance materials.

Effective design and optimization of these experimental platforms requires a strong synergy between the experimental program, condensed matter theory, magneto-hydrodynamic (MHD) simulation and electromagnetic modeling. Several individuals have contributed over roughly the last decade to transform the Z machine into a mature, robust, and precise platform for performing material dynamics experiments in the multi-Mbar regime.

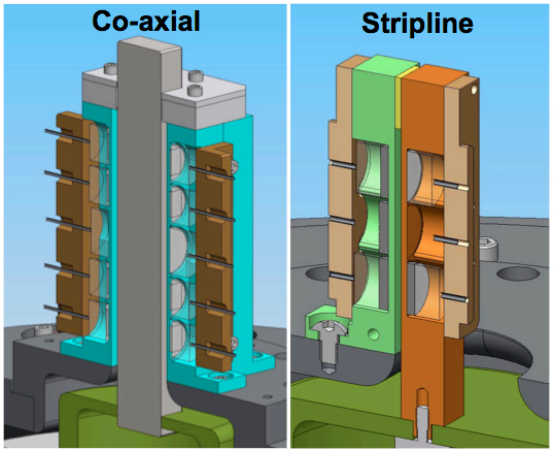

Figure 1. Co-axial and stripline configurations.

The intent of this paper is to provide a current snapshot of the material dynamics platforms on Z. In describing these platforms, attention will be drawn to the ways in which condensed matter theory, MHD simulation, and electromagnetic modeling have been used extensively in the design and optimization of these platforms. Finally, a few examples will be given to illustrate the close interplay between condensed matter theory and experiment, and how this interrelationship has challenged and advanced the capabilities of both experiment and theory.

RAMP COMPRESSION PLATFORM

As alluded to above, the stripline geometry has evolved to become the platform of choice for high-stress ramp compression experiments. This geometry all but eliminates the extremely restrictive alignment requirements of the coaxial load. However, the transition from a radial feed to a stripline feed is asymmetric, as can be seen in Fig. 1. For uniform width panels, this asymmetry results in magnetic field gradients up the length of

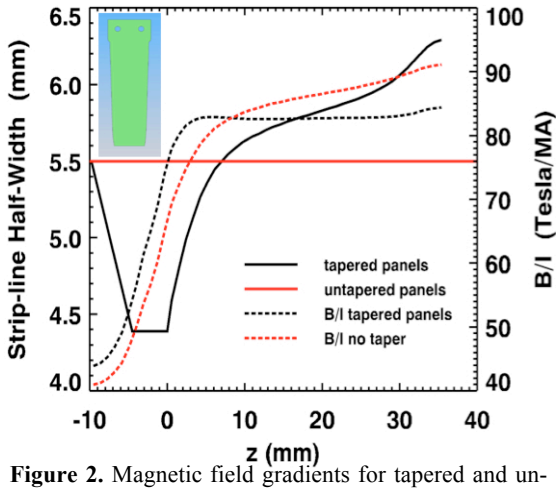

Figure 2. Magnetic field gradients for tapered and un-tapered panels as calculated by Emphasis. Inset shows isometric view of a tapered stripline panel.

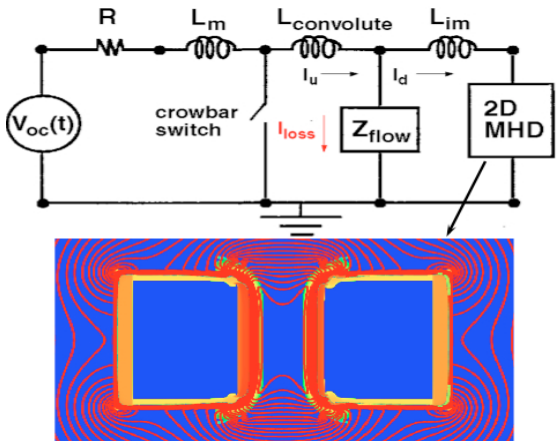

Figure 3. Circuit model for Z showing a 2-D MHD simulation as one of the circuit elements.

the stripline. Variable width, or tapered panels can be used to mitigate this pressure gradient.

To this end, 3-D transient electromagnetic simulations using Quicksilver and Emphasis [4] have provided optimization of the panel width as a function of height. Results of these simulations are shown in Fig. 2. Note that the initial field gradients are significantly reduced, from around 5-6% for un-tapered panels, to near zero for tapered panels. Experiments utilizing these tapered panels still show pressure gradients of a few percent, likely due to the fact that Quicksilver and Emphasis do not include dynamics, and thus the significant deformation which occurs during the current pulse is not accounted for. Nevertheless, experiments utilizing pairs of samples mounted on the anode and cathode directly opposite each other are not sensitive to the remaining gradient across the sample face (less than 1%). Furthermore, coupling of MHD simulations with the Quicksilver and Emphasis tools could continue to decrease the vertical gradients as the stripline platform evolves.

A predictive modeling capability is used to help guide the design and optimization of ramp compression experiments. Both one- and two-dimensional Eulerian simulation platforms have been developed using the finite element, arbitrary Lagrangian–Eulerian, MHD code ALEGRA [5] to solve the MHD equations for a compressible material with material strength. In these simulations, a complete equation of state valid for a wide range of pressures, densities, and temperatures is used for the conductor materials, in addition to physical models for thermal and electrical conductivities.

Initial ALEGRA simulations with existing Lee-More-Desjarlais (LMD) conductivity models for aluminum [6] proved to be inadequate. The simulations tended to over predict the extent of magnetic field diffusion into the electrode as compared to experimental measurement. This difference between simulation and observation resulted in a reinvestigation of the conductivity of aluminum, using quantum molecular dynamics (QMD) calculations [7]. It was found that the existing LMD model predicted too low a conductivity for liquid aluminum just beyond melt. ALEGRA simulations with a modified LMD model based on the QMD simulations showed much better agreement with experiment.

Two-dimensional MHD simulations are necessary to accurately predict load performance. Deformation of the load conductors, material motion, and Joule heating all result in an increase in the inductance and resistance of the load during the current pulse. Simulations must account for the coupling between the accelerator and the load in a self-consistent manner in order to accurately predict the drive current and the time-dependent loading profile of the stress wave. This is accomplished by coupling an accurate circuit

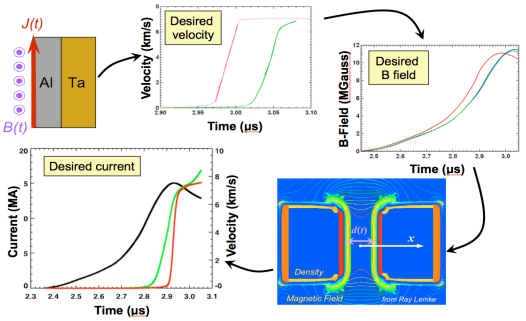

Figure 4. Schematic representation of experimental design using ALEGRA and DAKOTA.

model of the accelerator to the two-dimensional simulation of the load [3].

The specific circuit, shown in Fig. 3, includes equivalent resistances and inductances for the accelerator, as well as a time-dependent model of current loss and a time-dependent resistance that emulates a short circuit, both of which occur upstream of the MHD load. The inductance of the MHD load is calculated self-consistently in the simulation using an effective transverse length representative of the actual experimental load. Two-dimensional simulations using such a circuit model have been shown to accurately reproduce load performance for a variety of short circuit loads including both coaxial and stripline loads [3].

These ALEGRA simulations are invaluable for providing an accurate means to design and optimize ramp compression experiments. In particular, 1-D ALEGRA coupled with the optimization package DAKOTA [8] allow for optimization of electrode and sample thicknesses, and B(t) within the A-K gap that ensure (i) shockless compression of the samples, (ii) that reverberation of the elastic precursor from the sample/window interface does not reach the electrode/sample interface prior to peak stress, and (iii) that all samples experience the same stress loading history at the electrode/sample interface. 2-D ALEGRA simulations can then be performed to transform B(t) from the 1-D optimizations to an I(t) that accounts for deformation, material motion and Joule heating. This iterative approach to experiment design is illustrated in Fig. 4.

The example profiles shown in Fig. 4 are for the design of a ramp compression experiment on tantalum to ~400 GPa. 1-D ALEGRA simulations

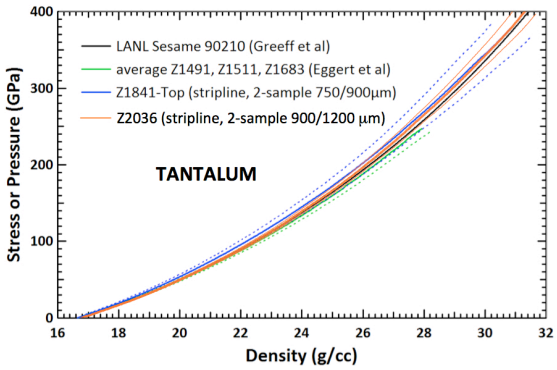

Figure 5. Quasi-isentrope of tantalum to over 400 GPa. Dashed lines indicate uncertainty bounds.

using an equation of state for tantalum from Carl Greeff [9] were used to optimize the B(t) necessary to produce the velocity profiles at the rear of 700 and 900 micron thick samples. 2-D ALEGRA simulations were then performed to determine I(t) for a 10 mm wide stripline geometry.

The machine configuration, including charge voltage, laser-triggered gas switch timings, and water switch gap settings, necessary to produce the required I(t) was determined using the Bertha code [10], a transmission-line circuit model for the Z machine. The Bertha code consists of over 3000 circuit elements, and continues to be refined to provide a predictive capability for pulse shaping required for material dynamics experiments.

In this way, quasi-isentropic compression data to ~400 GPa have been obtained for many materials, including aluminum, tantalum, copper, and gold. Figure 5 shows the result of several experiments on tantalum taken on Z over the past several years. The good agreement between the various experiments speaks to the consistency and repeatability of the Z platform for these types of experiments.

SHOCK COMPRESSION PLATFORM

The flyer plate platform was developed as an extension of the ramp compression platform, as it was realized that the magnetic pressure produced by the Z machine could be effectively used as an impulse to launch flyer plates to ultra-high velocities [3]. As such, the flyer plate platform has benefited from the advances that have allowed the

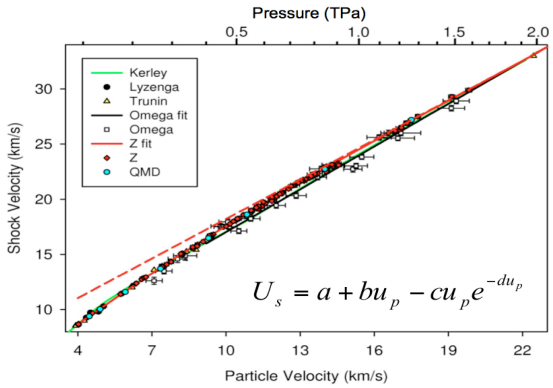

Figure 6. Hugoniot for alpha-quartz.

optimization of the ramp compression platform. In particular, the fully self-consistent, circuit representation of Z that includes the experimental load as one of the circuit elements has been invaluable in the maturation of this platform [3,11].

Over time, the coaxial geometry has evolved to become the load of choice for high-pressure shock compression experiments. In this case, the requirements for alignment between the anode and cathode can be relaxed. In other words, the advantage of this geometry fully containing the magnetic field outweighs the drawback of potential magnetic field gradients due to misalignment.

The default load geometry is a 9 by 2 mm cathode surrounded by a 17 by 4.4 mm anode. The cathode is offset within the anode, with 1 and 1.4 mm AK gaps. This results in differing peak magnetic pressures on the two sides of the load, which enables two different flyer velocities per firing of the Z machine. This capability enables 1 mm thick aluminum flyer plates to be launched to over 30 km/s.

The stripline geometry has also been explored as a means to reach even higher velocities. Recent experiments using a 10 mm wide stripline demonstrated flyer plate velocities in excess of 45 km/s (over 100,000 mph) [3]. Hugoniot measurements of both alpha-quartz and sapphire have been made at impact velocities over 40 km/s, producing Hugoniot pressures of ~16 and ~20 Mbar, respectively.

Composite flyer plates have also been developed to enable complex loading, such as shock and release for soundspeed measurements. In this case copper is electroplated onto aluminum and the plates are diamond turned to final dimensions of 750 and 150 microns of aluminum and copper, respectively. This process ensures a robust solid-state bound between the two metals.

Both experimental data and MHD simulations show that a significant portion of the original thickness of the flyer plate material remains essentially in the ambient state at impact. This enables the data to be analyzed simply with impedance matching considerations. Further details concerning the state of the flyer at impact can be found elsewhere [11].

As an example of the flyer plate technique, over 200 Hugoniot points for alpha-quartz, obtained with both aluminum and copper flyer plates, are shown in Fig. 6. These data, in conjunction with QMD calculations for quartz, have provided a new understanding of quartz in the multi-Mbar regime. In particular, it appears that the dissociation of quartz extends over a range spanning nearly 100-1000 GPa, much larger than previously expected [12]. This is significant given the prolific use of quartz as a standard in recent multi-Mbar experiments. In particular, the revision of this standard has resulted in corrections in the inferred density of deuterium of ~10-15% [12]. Even larger corrections may be necessary for higher compressibility materials such as helium [13].

EXAMPLES OF INTERPLAY BETWEEN THEORY AND EXPERIMENT

Over the past decade, a strong tie has been developed between the condensed matter theory and the experimental program. This coupling has been proven time and again to be extremely fruitful, with the capability of both theory and experiment being challenged and advanced through this close interrelationship. Two recent examples are noteworthy: beryllium and carbon. Both of these examples relate to work that was performed on the Z machine in support of the National Ignition Campaign for Inertial Confinement Fusion (ICF). In both cases the goal was to better understand the melt properties of these materials along the Hugoniot to aid in the design of ICF capsules and pulse shapes that would avoid the solid/liquid coexistence regime in the implosion of the capsule.

The first of these examples relate to the phase diagram of beryllium. In this case, the ability to obtain high precision experimental data in to multi-Mbar regime resulted in the re-evaluation of the phase diagram of beryllium using QMD calculations. The second example relates to the coexistence regime of carbon. In this case, high-fidelity QMD calculations guided the analysis of high-precision experimental data to provide evidence for the existence of a triple point in the coexistence region of carbon, and therefore the existence of a higher pressure phase of carbon beyond that of diamond.

Beryllium phase diagram

The widely accepted phase diagram for beryllium at the onset of this work was described by Sin'ko and Smirnov [14]. At ambient pressure and high temperature, just below melt, beryllium has been reported to undergo an hcp to bcc transition. Also, theoretical calculations suggested an hcp to bcc transition at zero K and high pressure. Thus it was assumed that these transition points were connected by a single phase boundary, at that the Hugoniot of beryllium would cross this phase boundary before encountering melt [14].

Based on this view of the phase diagram, QMD calculations were performed by both SNL [15] and LLNL [16] to determine the bcc melt boundary and the crossing of this melt boundary by the Hugoniot, to provide guidance for the experimental campaign. The SNL calculations suggested onset of melt at ~200 GPa. Thus a series of sound speed experiments utilizing composite aluminum/copper flyer plates were performed to investigate beryllium from ~150 to 350 GPa.

The details of the sound speed measurements will not be discussed here, however the concept is similar to that discussed by McQueen, et al. [17]. The results of these experiments are shown in Fig. 7. Also shown in Fig. 7 are the QMD predictions for sound speed in the bcc phase of carbon. Note the significant discrepancy between the longitudinal sound speed inferred from the bcc calculations and experiment. A similar difference was observed for the Hugoniot. This level of disagreement prompted a re-evaluation of the assumption regarding what phase beryllium melted from along the Hugoniot.

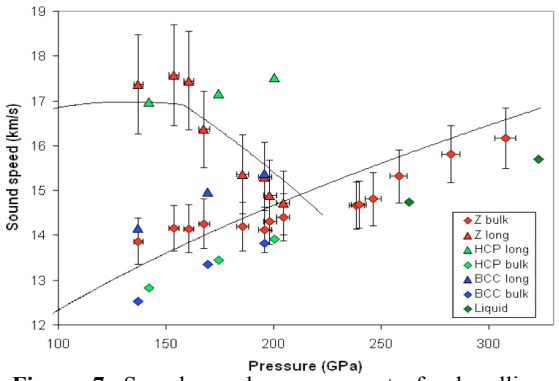

Figure 7. Sound speed measurements for beryllium along with QMD calculations for both bcc and hcp phases.

Subsequently a series of QMD calculations were performed to investigate the sound speed of beryllium in the hcp phase. These results are also shown in Fig. 7. Note the much improved agreement with respect to the longitudinal sound speed. Subsequent QMD calculations led to the prediction of an hcp-bcc-liquid triple point along the melt curve at a somewhat lower pressure than melt along the Hugoniot. A consequence of this would be that the Hugoniot first crosses the hcp-bcc transition at ~175 GPa, and then intersects the melt boundary at ~205 GPa. Note that the sound speed data is not inconsistent with this prediction – however, it is not proof of this transition. Clearly further study of the beryllium phase diagram is warranted and is planned in the near future.

Triple point along the coexistence curve for carbon

Not unlike the case of beryllium, little was known regarding the melting of carbon along the Hugoniot prior to this study. The only notable study was that by Bradley, et al. [18], who used the Omega laser to launch multi-Mbar, unsupported shock waves into diamond samples. These shock waves rapidly attenuated, and simultaneous measurements of the shock velocity and reflectivity were made. This study reported that carbon exhibited a rapid increase in reflectivity that started at ~600 GPa, and saturated at ~1100 GPa. They concluded that complete melt of carbon on the Hugoniot coincided with the observed saturation in reflectivity at ~1100 GPa.

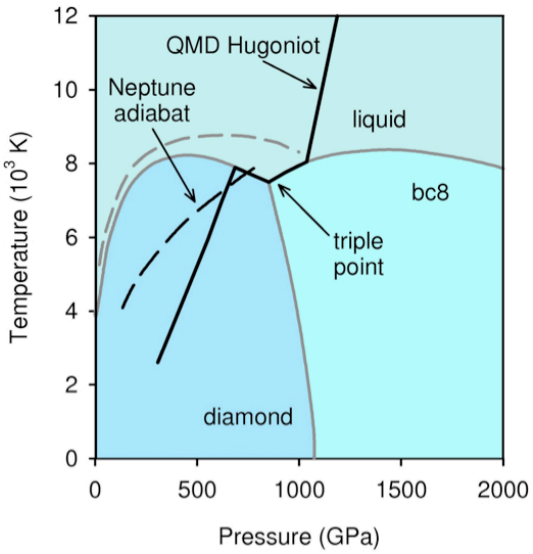

Figure 8. High pressure phase diagram for carbon.

Around the time of this study, a group at LLNL published a phase diagram for carbon based on QMD calculations [19]. Similar calculations at SNL corroborated the LLNL results, and furthered these results by focusing on the Hugoniot and its track through phase space. The resulting calculations suggested the coexistence region of solid and liquid carbon encompassed a diamond-liquid-bc8 triple point, as shown in Fig. 8 [20].

Detailed calculation of the Hugoniot in and near the coexistence region provided guidance for how the existence of a triple point would manifest itself in experimental observables. Notably, the QMD calculations predicted significant changes in the compressibility of diamond, diamond-liquid, bc8-liquid, and liquid carbon, with the changes in slope occurring at pressures of ~700, 875, and 1050 GPa, respectively, as shown in Fig. 9.

A series of 15 Hugoniot experiments were performed on Z in the pressure range of ~600 to 1400 GPa [20]. These data are shown in Fig. 9, along with the QMD predictions. As can be seen, the lowest and highest pressure data are in good agreement with the QMD calculations for the pure diamond and liquid phases. Furthermore, the data in the region of the predicted coexistence regime follow a similar trend to that of the QMD predictions.

Further analysis of the data considered two possible scenarios. First, the data was fit to a three

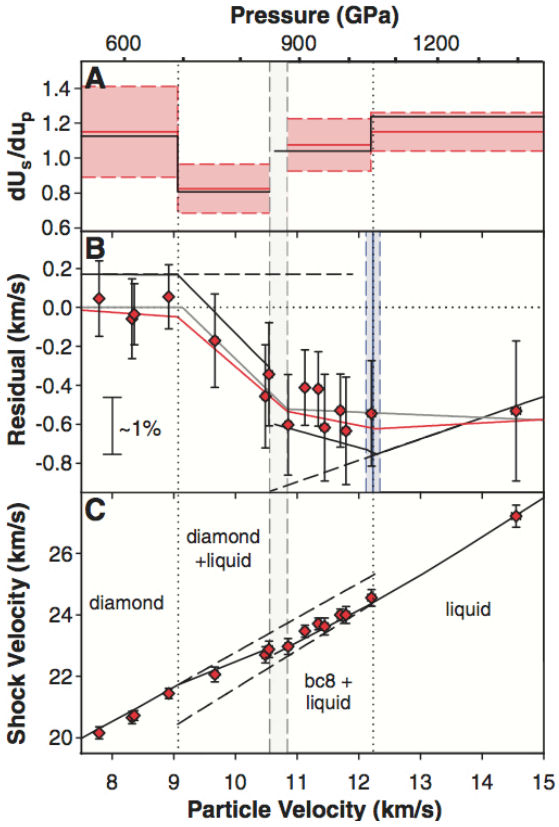

Figure 9. Hugoniot for diamond. **A** slopes, **B** residual plot with respect to the fit for solid diamond, **C** shock velocity vs. particle velocity. QMD results in black.

segment, piece-wise linear fit, which would be consistent with either the absence of the triple point, or relatively slow kinetics that prevented the observation of the triple point on the timescale of these experiments (several tens of ns). Second, the data was fit to a four segment, piece-wise linear fit, as suggested by the QMD calculations.

A Monte Carlo method was used in the fitting. The individual data points were randomly sampled within a population generated by the experimental values and uncertainties. A fit was then performed, and the slopes and breakpoints were recorded. This process was repeated for one million runs, and the slopes and breakpoints were obtained by determining the mean and standard deviations of the statistical populations. The results of both fits are shown in Fig. 9B.

Both fits are quite similar. In particular, both show significant changes in slope at pressures of

~700 and 875 GPa. Addition of a fourth segment results in an additional, relatively small slope change near ~1060 GPa. The three segment fit would suggest the onset and completion of melt at ~700 and ~875 GPa, respectively. However, this would be inconsistent with the results reported by Bradley, et al. [18]. The four segment fit, however, provides reconciliation with the Bradley results. In this case the initial large change in slope would correspond to onset of melt and the triple point, with the third change in slope, coinciding with the saturation in reflectivity, indicating the completion of melt.

CONCLUSIONS

Over the past decade the Z machine has been developed into a mature, robust, and precise platform for material dynamics experiments in the multi-Mbar regime. This has been the result of the work of a large interdisciplinary team that has effectively coupled condensed matter theory, MHD simulations, and electromagnetic modeling.

These tools will be used to continue to improve the capabilities at Z. In particular, effort is now on going to develop techniques to access regimes off the principal Hugoniot and off the principal isentrope utilizing multi-layered flyer plates and techniques to produce shock ramps. Finally, MHD simulations have paved the way to use convergent cylindrical imploding liners with x-ray radiography to increase the peak stresses for isentropic compression. Initial experiments on beryllium liners, which were reported on at this conference [21], indicate that with current backlighter energies (6.1 keV) the isentrope can be extracted to ~600 GPa. Higher energy backlighter energies could possibly extend these stresses to over 1 TPa.

ACKNOWLEDGEMENTS

Several colleagues and co-workers who have been invaluable members of the interdisciplinary team that has enabled the successes described here are gratefully acknowledged: Jim Asay, Rebecca Coats, Pat Corcoran, Devon Dalton, Jean-Paul Davis, Mike Desjarlais, Dan Dolan, Dave Funk, Rusty Gray, Carl Greeff, Tom Haill, Clint Hall, Heath Hanshaw, Dave Hinshelwood, William Langston, Keith LeChien, Ray Lemke, Matt Martin, Thomas Mattsson, Charlie Meyer, Ryan McBride, Paulo Rigg, Anthony Romero, Dustin Romero, Seth Root, Mark Savage, Dave Seidel, Brian Stoltzfus, Ken Struve, and the entire Z crew.

REFERENCES

1. Savage, M. E., et al., in Proceedings of the 2007 IEEE Pulsed Power Conference, Vols 1-4 (E. Schamiloglu, and F. Peterkin, eds.), pp 979-984 (2007).
2. Asay, J. R., in Shock Compression of Condensed Matter, 1999 (M.D. Furnish, L.C. Chhabildas, R.S. Hixson, eds.), pp 261-6.
3. Lemke, R. W., Knudson, M. D., and Davis, J.-P., Int. J. Impact Engng. **38**, pp 480-485 (2011).
4. Seidel, D. B., et al., in CP90 Europhysics conference on computational physics (A. Tenner, ed.), pp 475-482 (1991).
5. Summers, R. M., et al., Int. J. Impact Engng. **20**, pp 779-788 (1997).
6. Desjarlais, M. P., Contrib. Plasma Phys. **41**, pp 267-270 (2001).
7. Desjarlais, M. P., Kress, J. D., and Collins, L. A., Phys. Rev. E **66**, p 25401(R)-4 (2002).
8. Eldred, M. S., Giunta, A. A., and von Bloeman Waanders, B. G., Struct Multidisc Optim **27**, pp 97-109 (2004).
9. Greeff, C., private communication.
10. Struve, K. W., et al. in Proc. of the 2008 IEEE International Power Modulators and High Voltage Conference (H. Kirkici, ed.), pp 94-97 (2008).
11. Lemke, R. W., et al., J. Appl. Phys. **98**, pp 73530-9 (2005).
12. Knudson, M. D., and Desjarlais, M. P., Phys. Rev. Lett. **103**, pp 225501-4 (2009).
13. Eggert, J., et al., Phys. Rev. Lett. **100**, pp 124503-4 (2008).
14. Sin'ko, G. V., and Smirnov, N. A., Phys. Rev. B **71**, pp 214108-7 (2005).
15. Desjarlais, M. P., private communication.
16. Benedict, L. X., et al., Phys. Rev. B **79**, pp 064106-9 (2009).
17. McQueen, R. G., Hopson, J. W., and Fritz, J. N., Rev. Sci. Instrum. **53**, pp 245-250 (1982).
18. Bradley, D. K., et al., Phys. Rev. Lett. **93**, p 195506-4 (2004).
19. Correa, A. A., Bonev, S. A., and Galli, G., PNAS **103**, pp 1204-1208 (2006).
20. Knudson, M. D., Desjarlais, M. P., and Dolan, D. H., Science **322**, pp 1822-1825 (2008).
21. Lemke, R. W.; McBride, R., this proceedings.